IEEE Access
Multidisciplinary | Rapid Review | Open Access Journal

Received November 4, 2019, accepted November 21, 2019, date of publication November 25, 2019,
date of current version December 11, 2019.

Digital Object Identifier 10.1109/ACCESS.2019.2955555

Automated Detection of Myocardial Infarction Using a Gramian Angular Field and Principal Component Analysis Network

GONG ZHANG[1], YUJUAN SI[1,2], DI WANG[1], WEIYI YANG[1], AND YONGJIAN SUN[2]
[1]College of Communication Engineering, Jilin University, Changchun 130012, China
[2]Zhuhai College of Jilin University, Zhuhai 519041, China

Corresponding author: Yujuan Si (siyj@jlu.edu.cn)

This work was supported in part by the Key Scientific and Technological Research Project of Jilin Province under Grant 20170414017GH and Grant 20190302035GX, in part by the Natural Science Foundation of Guangdong Province under Grant 2016A030313658, in part by the Premier-Discipline Enhancement Scheme through the Zhuhai Government under Grant 2015YXXK02-2, in part by the Innovation and Strengthening School Project (provincial key platform and major scientific research project) through the Guangdong Government under Grant 2015KTSCX175, in part by the Premier Key-Discipline Enhancement Scheme through the Guangdong Government Funds under Grant 2016GDYSZDXK036.

ABSTRACT Myocardial infarction (MI) is a deadly disease that threatens human life worldwide, and it is essential to save threatened lives with early detection of MI. The electrocardiogram (ECG), which records the electrical activity presented in the heart, is used for the prevention and treatment of heart disease such as MI. However, it remains a challenge to visually interpret the ECG signals because of their small amplitude and duration. Inspired by the development in computer vision, we try to explore a novel approach for automatic detection of MI by imaging ECG signals without noise removal. In this paper, the ECG time series is first transformed into images using the Gramian Angular Difference Field (GADF) method. Subsequently, the processed images are subjected to the principal component analysis network (PCANet) to extract sparse high-dimensional features, which are easy to perform well in linear classifiers. We carried out several sets of experiments to test the effectiveness of our algorithm. The overall accuracy of 99.49%, the sensitivity of 99.78%, and the specificity of 98.08% are achieved in class-oriented experiments using original ECG beats. The accuracy even rises over 1% compared with the denoising one; Moreover, we also achieved favorable performance for the patient-specific experiment (accuracy of 93.17%, sensitivity of 93.91%, and specificity of 89.20%). The results of the experiments indicate that our model is an effective way to detect MI using raw ECG signals.

INDEX TERMS Electrocardiogram (ECG), myocardial infarction, Gramian angular difference field, principal component analysis network, patient-specific.

I. INTRODUCTION

Myocardial infarction (MI), caused by the interruption of blood flow in the myocardial segment [1], is one of the most common cardiovascular diseases. According to the American Health Association, approximately 720,000 Americans suffer from myocardial infarction each year [2]. Besides, myocardial infarction is often regarded as a silent heart attack because people do not realize that they have been suffering from myocardial infarction before the heart attack. Hence, it is crucial to accurately detect MI in the early stage of the disease, which can be achieved by electrocardiogram (ECG). An ECG is a noninvasive, economical, and primary tool to record the heart's electrical activity process, and it can provide a valuable reference value for the basic function of the heart and its pathological research. Generally, an ECG is the best way to measure and diagnose abnormal heart rhythms [3]. It consists of 12 leads (I, II, III, aVR, aVL, aVF, V1–V6), corresponding to special regions of the heart. The ECG lead V1, V2, V3, and V4 show the signatures of anterior MI and the inferior MI is diagnosed by ECG leads II, III, and aVF. The pathological characteristics of left lateral MI are observed from ECG lead I, aVL, V5, and V6 [5]. Besides, VCG has the advantage of recording

The associate editor coordinating the review of this manuscript and approving it for publication was Alicia Fornés.

electrical heart activities in three orthogonal planes (frontal, sagittal, and transverse) [11]. In recent years, most researchers used 12-lead ECG signals in their studies for myocardial infarction detection or localization [4]–[10]. Besides, several methods [11], [12] were reported for detection on the basis of vector electrocardiogram (VCG) signals. Almost certainly, different types of MI can be detected and distinguished by evaluating the alterations in different leads [13]. Most studies concentrate on traditional machine learning frameworks [4], [5], [6], [14]–[19]. For example, In [4], Arif et al. employed discrete wavelet transform (DWT) to extract features from the 12-lead ECG, and achieved the detection as well as the location of myocardial infarction using the k-nearest neighbor classifier. In [15], a new approach based on principal component multivariate multiscale sample entropy (PMMSE) is proposed. This model achieved an average accuracy of 90.34% using a least-square support vector machine classifier for the detection of cardiac diseases.

In general, all of the abovementioned methods have obvious drawbacks although they obtain acceptable performances. For one thing, there is room for further improvement in the achievements of MI detection. For another, due to external factors such as patient age and gender, the dominant or recessive ''features'' of the ECG change dynamically. Therefore, it is challenging to maintain generalization capabilities when using fixed hand-design features. Furthermore, several studies [6], [7], [20] listed in Table 9 have denoised the original signal in the preprocessing stage, resulting in additional time and memory consumption. Therefore, to overcome this limitation, deep learning frameworks have been introduced. Deep learning architectures such as deep neural networks [21], deep belief networks [22], recurrent neural networks [23] and convolutional neural networks (CNN) [24] have been applied to various fields. CNN is one of the most popular frameworks. It is most commonly used to analyze visual imagery and made remarkable achievements in the field of recommender systems [25],image classification [26], natural language processing [27], and medical image analysis. Several ECG analysis algorithms based on deep learning architectures have been developed recently [8], [28]–[34]. For instance, In the literature [8], the authors proposed a novel approach for MI detection using the Fourier-Bessel series expansion-based empirical wavelet transform (FBSE-EWT) and the deep layer least-square support vector machine (DL-LSSVM). The model achieved excellent performance (mean accuracy of 99.74%, the mean sensitivity of 99.87). Feng et al. proposed a hybrid model based on 16-layer CNN and long short-term memory networks (LSTM) for MI detection, and an accuracy of 95.4%, the sensitivity of 98.2%, the specificity of 86.5% were achieved [34].

It can be observed that deep learning models often achieve great performance because they have high-level structural features that can acquire the spatial and temporal characteristics of ECG signals [35]. However, the models mentioned require a considerable diversity of data and memory space due to the deep structures, which results in computationally expensive-to-learn features. Thus, some researchers are trying to use lightweight network models for ECG analysis. Chan *et al.* [36] proposed a novel, simple deep learning network called PCANet for image classification. This model can be efficiently designed to learn the features, and it has achieved great performance in image classification. Some researchers put forward their PCANet-based models for ECG application. For instance, Lee *et al.* [37] proposed a model based on PCANet to extract features for personal identification from the ECG Signal. PCANet is designed for multi-dimensional mode or image recognition applications. However, most researchers use the original one-dimensional ECG signal as the input to the PCANet, which doesn't fully utilize the time correlation of the original signal. We need to find an appropriate time series transformation approach to retain more ECG information. Some researchers also have carried out work for visual inspection [38], [39]. For instance, Silva *et al.* [38] extended the recurrence plot paradigm of time series classification using compression distance. Although these topological attributes improve classification performance, it is still unclear how these topological attributes relate to the original time series due to their inaccurate inverse operations.

Traditional machine learning methods may not acquire the generalized characteristics of ECG signals, while CNN consumes considerable diversity of data and memory space. To address the limitations above, we propose a novel and lightweight model based on GAF and PCANet for MI detection. The GAF method has a clear physical meaning for mapping from a time series to an image and can restore the original time series through the image. By using the lightweight framework, we can mine more useful components from the transformed ECG images, and export sparse high-dimensional features, which are easy to perform well in linear classifiers. The experimental results indicate that our proposed model can take into account performance and computation time, and achieve good performances for both class-oriented and patient-specific experiments.

A. GOALS

The main goals of the paper can be summarized as follows:

Goal 1: Develop an accurate and lightweight model for the automatic recognition of MI, which is robustness to noise.

Goal 2: Obtain more discriminative information from the original heartbeats by ECG time series transformation.

Goal 3: Design and realize the generalized algorithms for discriminating inter-patient variability.

B. NOVELTY AND ARRANGEMENT

Based on literature review such as Refs. [4], [5], [34], [40]; it can be summarized that the innovative elements of this study are as follows:

N1:Combination of ECG imaging method and high-level features extraction model: To take advantage of visually interpreting the ECG signals, a novel method (GADF) is

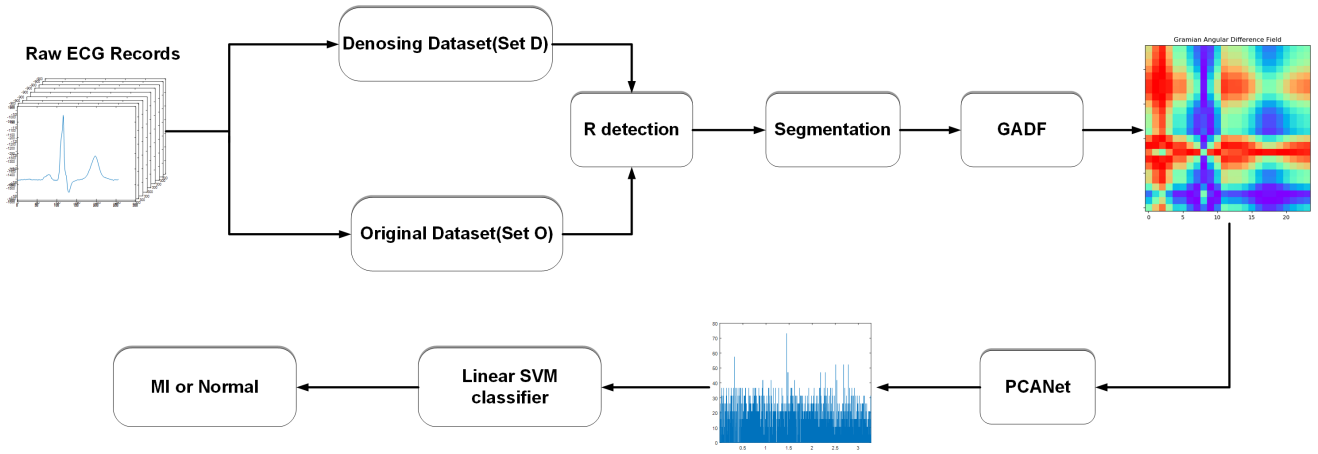

FIGURE 1. System sketch of the proposed system.

employed to transform the 1-D ECG signal to a 2-D image with significant information, and the lightweight CNN-like model(PCANet) is developed to obtain the high-level features from the processed image. The proposed model is proven to be an effective way to detect MI.

N2: Robustness to noise: Comparison experiments between denoising and original ECG signals are implemented. The results indicate that our model develops robustness of anti-noise.

N3: High accuracy: Compared with other literature, we achieved an excellent and stable performance in class-oriented experiments of MI detection.

N4: Generalization for patient-specific features: The patient-specific framework is adopted, and the proposed model can be adapted to learn the unique features from a specific patient, limiting the impact of inter-patient variability to an acceptable range.

The remainder of this paper is organized, as follows. Section II briefly introduces the database used in this paper and explains the basic theory of the proposed framework, including pre-processing, feature extraction (GADF and PCANet), and classification. The experimental results and discussion are shown in Section III and IV. Finally, Section V concludes the paper.

II. MATERIALS AND METHODOLOGY

A. MATERIALS

For this study, the ECG signals are obtained from the Physikalisch-Technische Bundesanstalt (PTB) diagnostic database [41]. The database contains 549 records from 290 subjects which include 209 men and 81 females, with ages ranging from 17 to 87. Each subject is represented by one to five records, and each record includes 15 simultaneously measured ECG signals. In this paper, we use only lead II for MI classification and aim to discriminate between healthy control and myocardial infarction. Specifically, we use 368 ECG records with MI, 80 ECG records with Healthy Control (HC). All the beats (10289 normal ECG beats, and 50486 MI ECG beats) are segmented by the QRS-wave detection. In particular, each beat is composed of 625 samples, including 249 samples before the R-peak point and 400 samples after the R-peak point. Demographical and statistical information on the dataset using the selection criteria from above is compiled in Table 1.

TABLE 1. Heartbeat category as per three assessment schemes.

Item	Normal (HC)	MI	Total
Subjects	52	148	200
Number of males	39	110	149
Number of females	13	38	51
Records	80	368	448
Number of heartbeats	10289	50486	60775

B. METHODS

The system sketch of the proposed methodology is shown in Figure 1. The system consists of four steps, which are described in pre-processing, imaging ECG time series, PCANet, and classification. The function of pre-processing is to obtain the heartbeats with noise and without noise. Next, we transform heartbeats into images using the GADF method. Finally, these processed images are subjected to the PCANet to extract sparse high-dimensional features, which are easy to perform well in linear classifiers such as Linear SVM. Close collaboration among these steps is desirable. The working of each block is explained in detail in the following sections.

1) PRE-PROCESSING

The original ECG signals with noise obtained from the PTB database. In this work, the orthogonal experiment has been designed using two sets of ECG data to test our proposed idea. Both datasets are composed of all original ECG signals and marked as set O (original) and set D (denoising). The related experiments are performed independently.

a: DENOISING

The noise of the ECG signals exists because of several factors, such as the DC bias drift of the ECG amplifier and the change in the resistance of the electrodes during recording

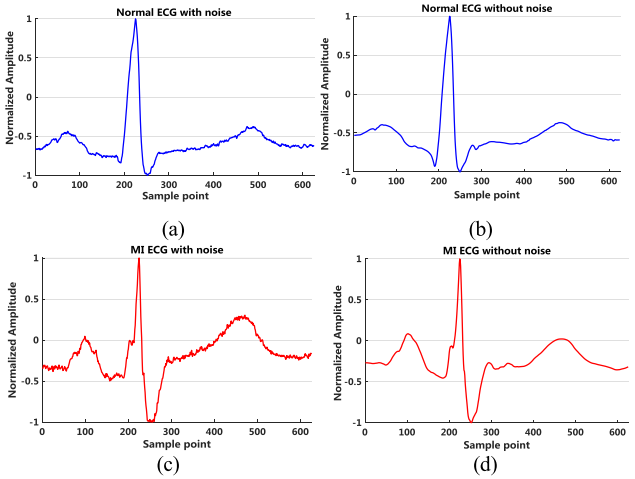

FIGURE 2. Comparison of normal and MI ECG beat (a) Normal ECG with noise; (b) Normal ECG without noise; (c) MI ECG with noise; (d) MI ECG without noise.

ECG signals [42]. Several methodologies have been proposed for ECG signal denoising, such as Spectro-temporal filtering [43], Wavelet-based filtering [44], eigenvalue decomposition of Hankel matrix [45], and so on. In this paper, we use the Daubechies wavelet eight mother wavelet function [46] to remove the baseline wander and high-frequency noises from the ECG signal for set D, set O remain the noise. Figure 2 shows details of a normal and MI heartbeat with and without noise.

b: BEATS SEGMENTATION

Second, comes the heartbeats segmentation phase. The Pan Tompkin algorithm [47] is used to carry out the R-peak point for both datasets, and the ECG signals are segmented for each heartbeat through the R-peak we detected, then the heartbeat segmented shall be normalized by min-max normalization method. In all, 60,775 heartbeats are acquired in each set.

2) IMAGING ECG TIME SERIES

The method called Gramian Angular Summation/Difference Fields (GASF/GADF) is adapted to encode ECG time series as images to take advantage of visually interpreting the ECG signals, in which a 1-D signal can be represented as a form of 2-D data [48], [49]. The step-by-step instructions are shown in Figure 3. The first step is to represent time series in a polar coordinate system by encoding the value of the ECG time series as the angular cosine and the time stamp as the radius. This procedure can preserve temporal dependency, then calculate its GASF/GADF images according to the defined GAF formula.

Specifically, the ECG time series $X = \{x_1, x_2, \ldots, x_n\}$ is scaled with a Min-Max scaler onto [−1,1] or [0,1]by:

$$\tilde{x}^i_{-1} = \frac{(x_i - \max(X)) + (x_i - \min(X))}{\max(X) - \min(X)} \tag{1}$$

$$\text{or } \tilde{x}^i_0 = \frac{x_i - \min(X)}{\max(X) - \min(X)} \tag{2}$$

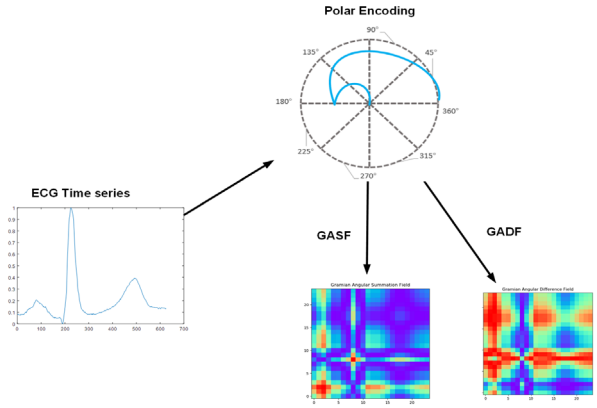

FIGURE 3. Illustration of the encoding map of Gramian Angular Fields.

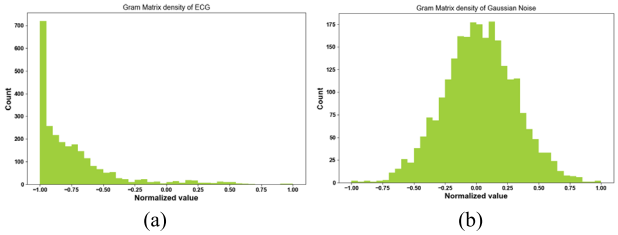

FIGURE 4. The density histograms of the outputs of the GAF Matrix. (a) ECG; (b) Classical Gaussian Noise.

Next, the rescaled time series $\tilde{X}$ in polar coordinates can be shown by encoding the value as the angular cosine and the time stamp as the radius by the equation below:

$$\begin{cases} \phi_i = \arccos(\tilde{x}_i), & -1 \le \tilde{x}_i \le 1, \tilde{x}_i \in \tilde{X} \\ r_i = \dfrac{t_i}{N}, & t_i \in \mathbb{N}, \end{cases} \tag{3}$$

where t_i is the time stamp and N constant factor to regularize the span of the polar coordinate system. In simple terms, we divide the interval $[0, 1]$ into N equal parts and therefore obtain $N + 1$ delimiting points $\{0, \ldots, 1\}$, then discard 0 and associate consecutively these points to the time series. Finally, after converting the rescaled time series into the polar coordinate system, we can use the angular perspective by considering the trigonometric sum/difference between each point to identify the temporal correlation within different time intervals, and the GAFs are defined as follows:

$$\begin{aligned} GASF &= \left[\cos\left(\phi_i + \phi_j\right)\right] \\ &= \tilde{X}' \cdot \tilde{X} - \sqrt{I - \tilde{X}'^2} \cdot \sqrt{I - \tilde{X}^2} \end{aligned} \tag{4}$$

$$\begin{aligned} GADF &= \left[\sin\left(\phi_i - \phi_j\right)\right] \\ &= \sqrt{I - \tilde{X}'^2} \cdot \tilde{X} - \tilde{X}' \cdot \sqrt{I - \tilde{X}^2} \end{aligned} \tag{5}$$

where I is the unit row vector, $\tilde{X}'$ and $\tilde{X}$ represent different row vectors. From the equations above, we notice that the GAFs are the newly constructed operation that corresponds to a penalized version of the conventional inner product.

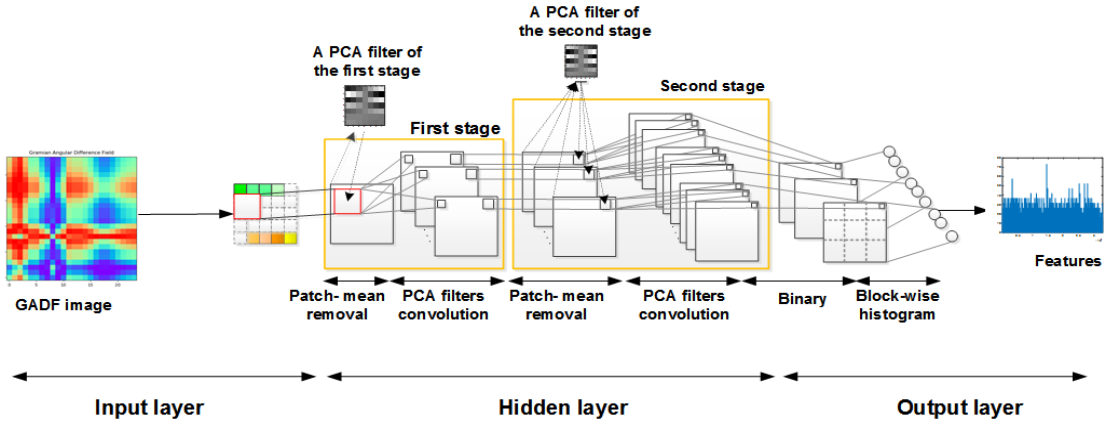

FIGURE 5. A detailed block diagram of the PCANet model.

GAF has several advantages. On the one hand, we plot the density of the Gramian Angular Field ECG values as shown in Figure 4. The density of GAF Matrix density of ECG is sparse, and its distribution is different from Gaussian Noise. Hence, the outputs are easily distinguishable from Gaussian Noise. On the other hand, we will approximately reconstruct the time series from the high-dimensional features. Moreover, temporal correlations are accounted for with the relative correlation by superposition/difference of directions concerning the time interval [48].

In this paper, our practical experience suggests that the GADF is more suitable for the ECG time series.

3) FEATURE EXTRACTION (pcanET)

In this section, ECG images processed are subjected to Principal Component Analysis Network (PCANet) model to obtain high-dimensional features. The PCANet framework can be considered as a simplified version of CNN for image classification, and it does not need a complicated iterative process for numerous parameters optimization. The training process of PCANet is more straightforward and faster than CNN. Vast experiments demonstrate the effectiveness of the PCANet in learning robust invariant features for different image classification tasks. The detail of the PCANet model is illustrated in Figure 5. PCANet is composed of three layers: the input layer, the hidden layer, and the output layer, including cascaded principal component analysis (PCA), binary hashing, and blockwise histograms. The most important part is the PCA filters. We firstly carry out the covariance matrix of the input training images. Then, we extract the first K eigenvectors with the highest energy using the PCA algorithm. Next, we stack these eigenvectors into a matrix, defined as PCA filters or convolution filters. The filters can capture the main variation of the original input. This is followed by simple binary hashing and block histograms for indexing and pooling. We binarize these outputs and view them as a decimal number. Eventually, we compute the histogram of the decimal values as the outputs of the framework. In what follows, we more precisely describe each component of the block diagram.

a: INPUT LAYER

There are N input ECG images $\{I_i\}_{i=1}^{N}$ of size m × n obtained in the previous step, and we suppose that the filter size is $k_1 \times k_2$ at all stages. Equation (6) shows that the matrix form of the $i-th$ image.

$$I_i = \begin{bmatrix} \mathrm{i}_{11}, i_{12}, \cdots i_{1n} \\ i_{21}, i_{22}, \cdots i_{2n} \\ \cdots \\ i_{m1}, i_{m2}, \cdots i_{mn} \end{bmatrix} \tag{6}$$

where m, n represents the width and height of the image, respectively.

b: HIDDEN LAYER

This layer consists of two stages from Figure 5. In the first stage filter extraction, we take the filter patch to slide with one step to select local features of the image, and the boundary of I_i is zero-padded before convolving with the $k_1 \times k_2$ filter to collect $m \times n$ patches of the $i-th$ image,i.e., $x_{i,1}, x_{i,2}, \ldots, x_{i,mn} \in \mathbb{R}^{k_1 k_2}$. Next, we remove the patch mean from each patch and combine these vectors to obtain $\bar{X}_{\mathrm{i}} = \left[\bar{x}_{i,1}, \bar{x}_{i,2} \ldots, \bar{x}_{i,mn}\right]$, where $\bar{x}_{i,j}$ is a mean-removed patch. All input ECG images are transformed into the same matrix via the same way, and we obtain

$$X = \left[\bar{X}_1, \bar{X}_2, \ldots, \bar{X}_N\right] \in \mathbb{R}^{k_1 k_2 \times Nmn} \tag{7}$$

We collect the PCA filters according to the PCA algorithm, and the PCA filters can be formulated as

$$W_l^1 = mat_{k_1,k_2}\left(q_l\left(XX^T\right)\right) \in \mathbb{R}^{k_1 \times k_2}, \quad l = 1, 2, \ldots, L_1 \tag{8}$$

Here, L_i represents the number of filters, and $q_l\left(XX^T\right)$ extracts the $l-$ th principal eigenvector of XX^T, $mat_{k_1,k_2}(v)$ is a function converting column vectors to matrices, so W_l^1 is the $l-$ th PCA filter to extract high-dimensional features for the first stage.

We obtain the $l-$ th filter output of the first stage by convolving the $l-$ th PCA filter with the input image I_i

$$I_i^l \doteq I_i * W_l^1, \quad i = 1, 2, \ldots, N \tag{9}$$

where I_i^l also have the same size as I_i because it is zero-padded before convolving with W_l^1.

As in the first stage, we repeat the same process: collect all patches of I_i^l, subtract the patch mean from each patch, and obtain $\bar{Y}_i^l = \left[\bar{y}_{i,l,1}, \bar{y}_{i,l,2}, \ldots, \bar{y}_{i,l,mn}\right] \in \mathbb{R}^{k_1 k_2 \times mn}$, where $\bar{y}_{i,l,j}$ is the $j-th$ mean-removed column vector of I_i^l, then we acquire $Y^l = \left[\bar{Y}_1^l, \bar{Y}_2^l, \ldots, \bar{Y}_N^l\right] \in \mathbb{R}^{k_1 k_2 \times Nmn}$ for the matrix and combine all $l-$ th filter output to achieve

$$Y = \left[Y^1, Y^2, \ldots, Y^{L_1}\right] \in \mathbb{R}^{k_1 k_2 \times L_1 Nmn} \tag{10}$$

The next step is to apply PCA algorithm to get the PCA filters of the second stage,

$$W_\ell^2 = mat_{k_1,k_2}\left(q_\ell\left(YY^T\right)\right) \in \mathbb{R}^{k_1 \times k_2}, \quad \ell = 1, 2, \ldots, L_2 \tag{11}$$

Each input I_i^l of the second stage will output L_2 images of the size of $m \times n$ according to the equation (12)

$$\mathrm{O}_i^l \doteq \left\{I_i^l * W_\ell^2\right\}_{\ell=1}^{L_2}, \tag{12}$$

where O_i^l is the output of the $i-th$ image, and the $L_1 L_2$ represents the number of output images.

c: OUTPUT LAYER

In this layer, the outputs of the second stage $\left\{I_i^l * W_\ell^2\right\}_{\ell=1}^{L_2}$ will be binarized, and then these binary matrices are converted to decimal matrices as

$$\Gamma_i^l \doteq \sum_{\ell=1}^{L_2} 2^{\ell-1} H\left(I_i^l * W_\ell^2\right) \tag{13}$$

where Γ_i^l is the $l-$ th decimal matrix for the $i-th$ image, and $H(\cdot)$ is a Heaviside step function, in which value is one for positive entries and zero otherwise. Each of the Γ_i^l, $l = 1, \ldots, L_1$ is divided into B blocks, and we calculate the histograms and concatenate all B histograms into one vector as $Bhist\left(\Gamma_i^1\right)$ the input image I_i is then converted to the set of block-wise histograms after this encoding process. We finally obtain the feature vectors as

$$f_i \doteq \left[Bhist\left(\Gamma_i^1\right), \ldots, Bhist\left(\Gamma_i^{L_1}\right)\right]^T \in \mathbb{R}^{(2^{L_2})L_1 B} \tag{14}$$

4) Classification

In this paper, we implement several standard classifiers such as Support Vector Machines [50], Linear Discriminant Analysis [51], back propagation neural network [52], k-nearest neighbor classifier and Random Forests [53] to evaluate the performance of our proposed model.

FIGURE 6. The impact of the image size(width=height).

5) K-FOLD CROSS-VALIDATION

In recent years, k-fold cross-validation is commonly used in applied machine learning to compare and select a model for a given predictive modeling problem. It is easy to understand and implement, resulting in the skill estimates that generally have a lower bias than other methods. In our experiment, the data was partitioned into k(k=5) equal-sized parts. Unlike the conventional one, one of the five parts was selected for training and the remaining data for testing at each iteration. Although only one-fold data was used for training, we achieved good results. The final results recorded in all five iterations are averaged and considered as the overall performance of our proposed system. For all class-oriented experiments, we used this cross-validation method.

6) EVALUATION CRITERIA

The equations for the calculated coefficients are as follows:

- **Accuracy**

$$ACC = \frac{TP + TN}{TP + FP + TN + FN} \tag{15}$$

- **Sensitivity**

$$SEN = \frac{TP}{TP + FN} \tag{16}$$

- **Specificity**

$$SPE = \frac{TN}{FP + TN} \tag{17}$$

- **Positive Predictive Value**

$$PPV = \frac{TP}{TP + FP} \tag{18}$$

where TP means detection correctly with the disease, TN is being identified as correctly without the disease, FN means detection incorrectly when the disease is present, and the detector is not detected, FP means the disease is not present, but detector detects disease.

III. EXPERIMENT RESULTS

A. MODEL STRUCTURE AND PARAMETERS

In this paper, a novel model, with feature extractions, including imaging ECG time series and PCANet, is developed.

First, we represent time series in a polar coordinate system to preserve temporal dependency, and then calculate its GADF images, which are subjected to PCANet framework to obtain sparse high-dimensional features; eventually, the features are fed to the linear SVM classifier to get the final label. For optimizing the parameters of the structure, several experiments were performed on the validation set to investigate the impact of the size of images, the number of filters, and different block sizes for the proposed model. According to the analysis results above, we set a series of regular parameter values and then use a grid search algorithm to find the optimal combination of parameters. We used 2000 instances as the validation set and employed the 5-fold cross-validation for each iteration. To demonstrate the advantages of our model, we conducted several contrastive experiments. Moreover, we then compared the proposed model with state-of-the-art methods on all test sets. All the experiments were implemented in Matlab R2018a and Pycharm 2018 on a Windows 7 with Intel Core i7 CPU(@2.60GHz) and 8GB RAM.

1) IMPACT OF THE SIZE OF IMAGES

As mentioned above, each heartbeat consists of 625 samples, which can be folded into a senseless image (25×25). Hence, we varied the size of the output image from 25×25 to 60×60 for evaluating performance; then we fixed other parameters (the filter size $k1 = k2 = 5$, the number of the filter $L1 = L2 = 5$, and the block size $b1 = b2 = 4$). The results are presented in Figure 6. One can observe that the accuracy of the model approximately increases with the rise of the image size, and the model achieves the best results when the size of the image is close to 50×50. Moreover, the high dimension of the feature space decreases the accuracy rate and sacrifices performance when the size of the image $I > 50 \times 50$.

2) IMPACT OF NUMBER OF FILTERS

In this subsection, we designed two groups of experiments. Firstly, we fixed the size of input images $I = 25 \times 25$, the filter size of the network $k1 = k2 = 5$, and the block size $b1 = b2 = 4$. For one experiment, we controlled the number of filters in the second stage $L2 = 5$, and changed the number of filters in the first stage $L1$ from 2 to 16; For another experiment, we fixed $L1 = 5$ and varied the number of filters in the second level $L2$ from 2 to 16. Figure 7 shows the accuracy for each epoch. The results suggest that the accuracy increases for larger $L1$ or larger $L2$, and the effect on the performance of $L1$ is more significant than the other. It's not difficult to see the model achieves the best accuracy when $L1$ approaches 6 or $L2$ is close to 8.

3) IMPACT OF BLOCK SIZE

Similarly, we test the impact of block size on accuracy. The results are presented in Figure 8. Note that the model achieves the best accuracy when $b1$ approaches 5 or $b2$ is close to 5, and the accuracy starts to show a decreasing trend when $b1 > 5$ or $b2 > 5$.

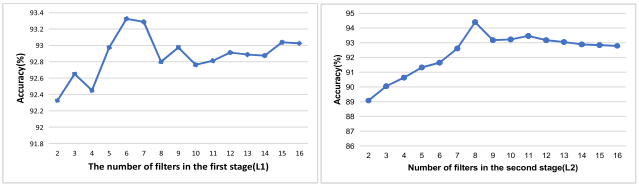

(a) (b)

FIGURE 7. The impact of the number of filters. (a) The first stage; (b) The second stage.

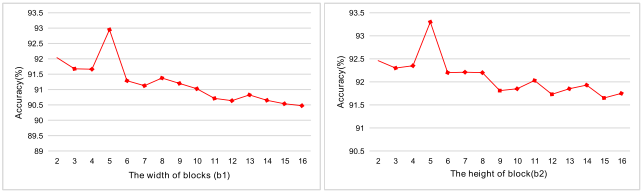

(a) (b)

FIGURE 8. The impact of the number of the block size. (a) The width; (b) The height.

TABLE 2. Alternative grid parameter list and the optimal combination of parameters for our model.

Project	Parameters	Alternative List	Best
GADF	Image_size	[25×25,...,60×60]	50×50
PCANet	Patch Size	[5×5,7×7,9×9]	7×7
	Number of filters in the first stage	[4,5...,9]	5
	Number of filters in the second stage	[4,5...,9]	5
	The block size	[3×3,3×4,...,7×7]	7×5

4) GRID SEARCH ALGORITHM

As shown in Table 2, we set the alternative grid parameters based on the analysis above and find the best combination of settings.

B. CLASS-ORIENTED EXPERIMENTS OF MI DETECTION

In this subsection, the original dataset (set O) with noise was used for class-oriented experiments of MI detection. Before the cross-validation was employed for performance evaluation, the heartbeats from set O were randomly scrambled. All heartbeats were departed almost equally into five segments. For each iteration, 1/5 heartbeats were selected for training while the remainder(4/5) were used for testing. The approach was repeated five times by shifting the testing part. The confusion matrix of each fold for MI detection is shown in Table 3.

We discover that our algorithm achieved significantly competitive results on MI detection based on Table 3. The overall accuracy, positive predictive value, and sensitivity are 99.49%, 99.61%, and 99.78%, respectively. Furthermore,

TABLE 3. The results of each fold for class-oriented experiments of MI detection.

Fold	Actual \ Predicted	Normal	MI	ACC(%)	PPV(%)	SEN(%)	SPEC(%)
1	Normal	8030	156	99.47	99.61	99.75	98.09
	MI	100	40334				
2	Normal	8063	171	99.47	99.58	99.79	97.92
	MI	85	40301				
3	Normal	8070	172	99.46	99.57	99.77	97.91
	MI	92	40286				
4	Normal	8139	159	99.50	99.61	99.79	98.08
	MI	83	40239				
5	Normal	8064	132	99.55	99.67	99.79	98.39
	MI	86	40338				
Overall	Normal	40366	790	99.49	99.61	99.78	98.08
	MI	446	201498				

TABLE 4. The overall classification results for MI detection classes using ECG beats with and without noise.

Beats type	TP	TN	FP	FN	ACC(%)	PPV(%)	SEN(%)	SPEC(%)
Noise	201498	40366	790	445	99.49	99.61	99.78	98.08
Without Noise	200315	38986	2170	1629	98.44	98.93	99.19	94.73

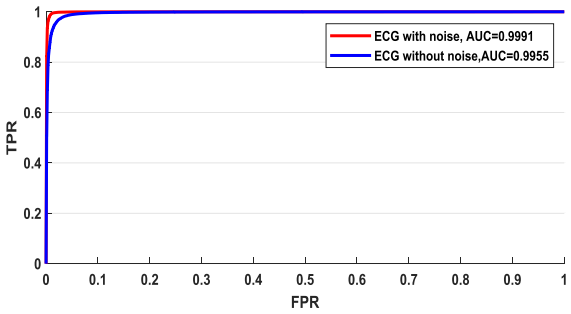

FIGURE 9. The ROC curves of the ECG with noise and without noise.

the variation of the three indicators is <0.2%, which demonstrates our method is sufficiently stable and can accurately perform class-based MI detection.

C. COMPARISON EXPERIMENTS OF DENOISING AND ORIGINAL DATA

In this subsection, we conducted contrast experiments using the denoising dataset (set D). The overall confusion matrix for heartbeats with and without noise is shown in Table 4, and the Receiver Operating Characteristic (ROC) curves are depicted in Figure 9. As can be seen from Table 4, an overall accuracy, positive predictive value, sensitivity, and specificity of 98.44%, 98.93%, 99.19%, and 94.73% are achieved, respectively. It turns out that even the experiments using heartbeat with noise show a significant rise on accuracy (98.44%∼99.49%), positive predictive value (98.93%∼ 99.61%), sensitivity (99.19%∼99.78%) and specificity (94.73%∼98.08%). The AUC of the model with noise just achieved a slightly higher AUC than the denoising one (0.9991>0.9955). In general, our proposed model is robustness to noise.

TABLE 5. The optimal parameter values of different classifiers.

Classifier	Parameters	Value
KNN	The number of neighbors	3
BP	Hidden layer size	50
RF	The number of decision trees	500
LDA	DiscrimType	pseudolinear
SVM-RBF	BoxConstraint (gamma)	0.5
	The punish coefficient (C)	1
SVM-Linear	The punish coefficient (C)	1

D. COMPARISON EXPERIMENTS OF DIFFERENT CLASSIFIERS

Several typical classifiers were involved in heartbeat classification in this paper. The optimal parameters of all classifiers were set to the values as in Table 5. The results of 5-fold cross-validation are shown in Table 6, and the associated box

TABLE 6. The accuracy of different classifiers across 5-fold.

Classifier	Fold1	Fold2	Fold3	Fold4	Fold5	OA
KNN(%)	98.14	98.12	98.10	98.04	98.19	98.12
BP(%)	99.10	99.05	98.70	98.78	98.76	98.88
RF(%)	98.78	98.80	98.72	98.70	98.64	98.73
LDA(%)	99.41	99.47	99.42	99.36	99.37	99.41
SVM-RBF(%)	99.48	99.42	99.38	99.48	99.45	99.44
SVM-Linear(%)	99.47	99.47	99.46	99.50	99.55	99.49

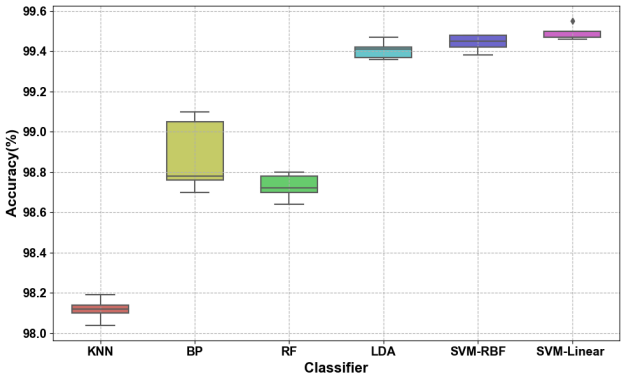

FIGURE 10. The accuracy box plot of different classifiers.

plot is shown in Figure 10 to display the influences of different classifiers on the accuracy of classification results. One can conclude each classifier has high accuracy (approaching 99%) because of the distinguishable feature extracted in the previous stage of work. As for the stability of the proposed model, the difference in overall accuracy is minuscule (1%). Obviously, the linear SVM classifier obtains the highest overall accuracy (99.49%). Also, it can be seen that the accuracy of BP changes more slightly than the other classifiers. That's because the weights and thresholds are randomly given when the BP nets start training.

To sum up, the proposed model with general applicability has good performances on several classifiers. One explanation could be that GADF represents the ECG signal in a polar coordinate system to preserve temporal dependency because time increases as the position moves from top-left to bottom-right [48]. Temporal dependency played a major role in extracting the multi-frequency dependencies through the convolution of PCA filters [54]. The high-dimensional features extracted from the GADF image are easy to perform well in linear classifiers.

E. PATIENT-SPECIFIC EXPERIMENTS

As we know, inter-patient variability is the main challenge of automatic analysis for ECG in real-world applications.

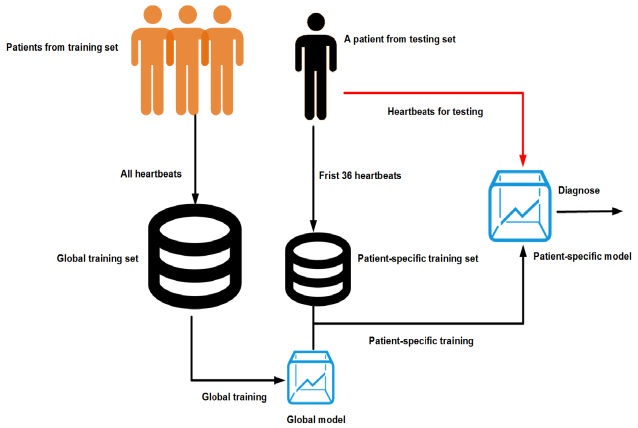

FIGURE 11. The patient-specific framework.

The models based on a fixed training set may fail to classify heartbeats from a new patient because of the unique physiological characteristics of each person's heart or ages, genders, and the patient's past medical history [55]. We employed the patient-specific framework aiming at the question. The main idea of the framework is that the data used to train the individual patient's classifier consist of two parts: global (common to all patients) and local (patient-specific) training datasets [56]. The model is first trained using a global dataset to get a relatively small number of representative heartbeats. Then, a patient-specific dataset from the new patient is used to perform patient adaptation. This framework has been proven to be feasible for identifying inter-patient variability. The patient-specific framework is illustrated in Figure 11.

In the patient-specific experiments, we employed traditional k-fold cross-validation to verify the reliability of the proposed method further. For the dataset partition, we divided all patients (not heartbeats) into five almost equal groups. Some 4/5 patients were selected as the global training set, while the remainder(1/5) of the patients were used as the testing set for each iteration. Subsequently, we only extracted the first 36 heartbeats from the testing of each patient as the patient-specific training set. The parameters of the model were the same as those in the class-oriented experiments.

The results of MI detection from the patient-specific experiments are shown in Table 7. Note that we achieved an accuracy of 93.17%, sensitivity of 93.91%, and specificity of 89.20%. The performance of the patient-specific model is significantly lower than the class-oriented experiments, which indicates that the inter-patient variability can reduce the generalization capacity and stability of the proposed model to a certain extent. Moreover, it can also be inferred that we achieve a good performance on fold 1, 4, and 5, but obtain a weak effect on fold 2 and 3. The reasons for this are attributed to two aspects. Firstly, fold 2 and 3 have fewer training samples (nearly 47000 heartbeats) than the other fold (approaching 52000 heartbeats) because the number of heartbeats for each patient is different in the PTB database. Secondly, the waveform of MI patients on fold 3 contains

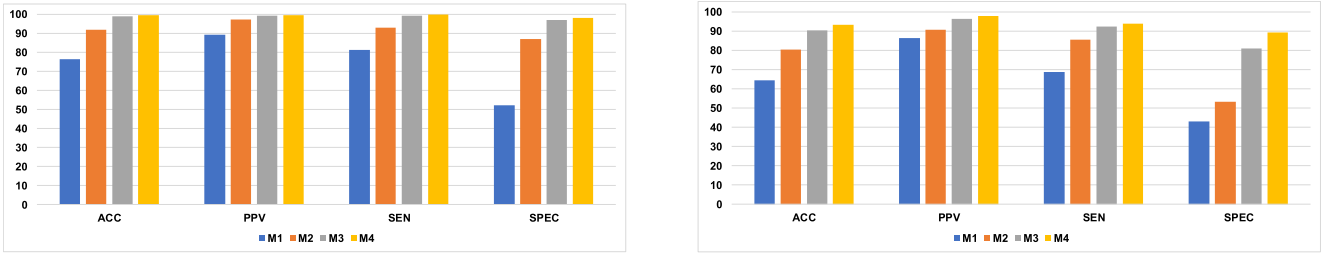

(a) (b)

FIGURE 12. The performance of different models for MI detection. (a). Class-oriented; (b). Patient-specific.

TABLE 7. The results of MI detection of the patient-specific experiments across 5-fold.

Fold	Predicted / Actual	Normal	MI	ACC(%)	PPV(%)	SEN(%)	SPEC(%)
1	Normal	1126	30	97.54	99.72	97.55	97.40
	MI	269	10711				
2	Normal	2010	238	91.71	97.91	92.13	89.41
	MI	951	11137				
3	Normal	1641	277	88.24	97.43	88.68	85.56
	MI	1340	10495				
4	Normal	1488	96	96.74	98.64	97.37	93.94
	MI	188	6953				
5	Normal	1275	272	94.10	92.04	99.84	82.42
	MI	5	3145				
Overall	Normal	**7540**	**913**	**93.17**	**97.89**	**93.91**	**89.20**
	MI	**2753**	**42441**				

much more noise, and it is more challenging to extract unique features from specific patients.

To summarize, although the performance of the patient-specific model is less than ideal, the proposed model can limit the impact of inter-patient variability to an acceptable range with the usage of the patient-specific framework.

F. COMPARISON EXPERIMENTS OF GADF AND PCANET

Comparative experiments were carried out using the original dataset to show the advantages of imaging ECG time series and PCANet. Table 8 and Figure 12 show the results of comparative experiments. By comparing the performance of M1 and M2 for class-oriented scheme, it can be observed that the approach shows better classification performance when the ECG time series is transformed into the images, which results in a significant rise on accuracy (76.38%∼91.93%), positive productivity (89.31%∼97.21%), sensitivity (81.29%∼92.95%), and specificity (52.25%∼ 86.90%). Also, we can see the performance improvement in each metric by comparing the performance of M3 and M4.

The same trend exists for the patient-specific scheme. Furthermore, the comparison between M1 and M3 shows that our model provides an overall performance boost for both the class-oriented and patient-specific scheme. Hence, the proposed model can efficiently get more information from the original heartbeats due to its good ability to feature learning.

IV. DISCUSSION

Comparisons with denoising experiments verify that our model is robustness to noise for MI detection. The reason is that the original signal has an inevitable overlap in the noise domain and the information domain. It may remove a small number of informative features when we use wavelet to denoise. Meanwhile, we can infer that the outputs of the GADF are easily distinguishable from Gaussian noise, so the PCA filters can remove useless noise from the original ECG signal and retain more useful information.

From Table 8, we can see that the PCANet model performs better than the GADF method. Moreover, we found an increment in the accuracy of classification when the model composed of PCANet and GADF is employed. PCANet is a CNN-like lightweight framework designed for extracting significant features from an image. To fully utilize the advantage of visually interpreting the ECG signals, we transform the ECG time-series into an image using the GADF method before being fed to the PCANet. The combination of both

TABLE 8. The results of comparative experiments for MI detection across 5-fold.

Scheme	Model	GADF	PCANet	Linear SVM	ACC(%)	PPV(%)	SEN(%)	SPEC(%)
Class-oriented	M1	N	N	Y	76.38	89.31	81.29	52.25
	M2	Y	N	Y	91.93	97.21	92.95	86.90
	M3	N	Y	Y	98.97	99.38	99.38	96.95
	M4 (Proposed Model)	**Y**	**Y**	**Y**	**99.49**	**99.61**	**99.78**	**98.08**
Patient-specific	M1	N	N	Y	64.55	86.53	68.59	42.93
	M2	Y	N	Y	80.40	90.72	85.48	53.27
	M3	N	Y	Y	90.56	96.30	92.34	81.05
	M4 (Proposed Model)	**Y**	**Y**	**Y**	**93.17**	**97.89**	**93.91**	**89.20**

M1 (Linear SVM): Heartbeats would be directly fed to the Linear SVM classifier to get the label.
M2 (GADF +Linear SVM): Heartbeats would be transformed into images by GADF before feeding to Linear SVM classifier.
M3 (PCANet +Linear SVM): Heartbeats would be folded into vectors heartbeat matrices as the input of PCANet, and then the outputs of PCANet would be sent to the classifier.
M4 (GADF+PCANet+Linear SVM): Heartbeats would be transformed firstly into a polar coordinate system, and then calculate its GADF images, which are subjected to PCANet to obtain high-dimensional features; eventually the features are fed to the classifier to get the final label.

TABLE 9. Performance comparison of the proposed method and other methods for MI detection using ECG signals obtained from the PTB database.

Author	Method	No. of Leads	MI detection	
			Class-oriented	Patient-specific
Sun et al.,2012[6]	SVM	12 leads	Sen =92.60% Spec=82.40%	NA
Safdarian et al.,2014[20]	Naïve Bayes	Lead II	Acc = 94 .74%	NA
Liu et al.,2015[10]	ECG polynomial fitting algorithm	12 leads	Acc = 94 .40%	NA
Sharma et al.,2015[5]	SVM	12 leads	Acc = 96.00% Sen = 93.00% Spec = 99.00%	NA
Acharya et al., 2016[7]	KNN	12 leads	Acc = 98.80% Sen = 99.45% Spec = 96.27%	NA
Acharya et al.,2017[40]	CNN	Lead II	Acc = 95.22% Sen = 95.49% Spec = 95.19%	NA
Feng et al.,2019[34]	CNN -LSTM	Lead I	Acc = 95.40% Sen = 98.20% Spec = 86.50%	NA
Proposed	GADF PCANet Linear SVM	Lead II	Acc = 99.49% Sen = 99.78% Spec= 98.08%	Acc=93.17% Sen=93.91% Spec=89.20%

can offer more sufficient information and further improve the prediction ability. Furthermore, the composed model can limit the impact of inter-patient variability to an acceptable range.

Table 9 summarizes the various techniques by which researchers use the ECG signals obtained from the PTB database to detect MI automatically. Note that lead II ECG signals were not used in all studies. Most researchers used 12-lead ECG signals in their studies for MI detection or localization. Although the multi-lead (12-lead or VCG-lead) can provide more comprehensive information and achieve good performance, the time complexity of the model also increases. In this paper, we aim to detect MI without the need for localization of MI. Hence, we only used lead II

because it is a common clue for necessary cardiac monitoring, and it could provide useful morphological information of ECG. The results of the experiments prove that we can achieve good performance by using only lead II. Moreover, the implementation with a single lead indicates the possibility of applications in mobile systems such as wearable or portable devices. It also can be noted from Table 9 that our proposed system performed better using the original ECG beats. In [40], the authors proposed a convolutional neural network (CNN) algorithm using lead II only for automated MI detection. Their model achieved acceptable performance using original ECG. However, the calculation cost of the 11-layer deep CNN is computationally intensive to learn the features. It can be seen that the deep learning method can achieve great performance, but deep learning models usually consume a lot of data and memory, leading to an increase in computational complexity. Compared with the deep learning framework, our proposed model has lower time complexity since the extracted PCA filters are directly used as convolution kernels for PCANet. It does not need to calculate convolution kernels like CNN through a complicated iterative process. The time-consuming operation of our proposed system mainly focuses on the convolution operation of PCANet and the training process of the SVM classifier. In a single CPU, the average time for one convolution operation of a heartbeat is about $0.4\mu s$. Considering a complete PCANet run with $30 \times 50 \times 50$ iterations($5 \times 50 \times 50$ in the first stage, $25 \times 50 \times 50$ in the second stage) over a training dataset with 48639 heartbeats (39506 MI heartbeats, 9133 HC heartbeats), which means that the average time for PCANet training would be $0.4 \times 30 \times 50 \times 50 \times 48639\mu s = 24.3$ min. The average time for SVM-Linear training is about 102s, and the average extraction and classification of a test ECG beat instance is about 19ms. In [7], the test time for a multi-lead ECG beat instance is 208.5ms. Note that the speed of our approach is acceptable.

The main advantage of the proposed approach is its robustness of anti-noise. We can obtain excellent performance using the original ECG signal without denoising. Then, the impact of inter-patient variability can be limited to an acceptable range due to the good generalization performance and sparsity of our proposed model. Furthermore, our proposed model has a lower time complexity compared with CNN. The main limitation of our model is the slightly larger memory requirement due to the sparse high-dimensional features of PCANet output.

V. CONCLUSION

In this study, we put forward a novel model to detect MI automatically on the PTB database. By using PCANet, the high-dimensional and generalized features were extracted from the images transformed by the GADF method. We achieved great performances on both class-oriented and patient-specific experiments. Specifically, by using the original ECG signals, the model achieved an overall accuracy of 99.49% for class-oriented experiments; the accuracy was even over 1% higher than the denoising one. Moreover, an overall accuracy of 93.17%, sensitivity of 93.91%, and specificity of 89.20% were obtained in the patient-specific experiments. The experimental results and analysis conclude that the proposed model has competitive performance when compared to the listed literature above. Hence, our proposed model can accurately detect MI from the unknown ECG signals even with noise. The proposed approach will be a useful component of the cardiologist's clinical decision support system.

Future work will be devoted to exploring a better model to improve the performance in the patient-specific experiments. This approach is also intended to extend to other cardiovascular diseases such as coronary artery disease, and congestive heart failure. The ultimate goal of this work is to design the cloud realization of the proposed method and apply it in mobile devices to provide a more reliable and practical diagnosis.

REFERENCES

[1] R. U. Acharya, N. Kannathal, L. M. Hua, and L. M. Yi, "Study of heart rate variability signals at sitting and lying postures," *J. Bodywork Movement Therapies*, vol. 9, no. 2, pp. 134–141, Apr. 2005.

[2] E. J. Benjamin, "Heart disease and stroke statistics-2017 update: A report from the American Heart Association," *Circulation* vol. 135, no. 10, pp. 146–603, Mar. 2017.

[3] P. Kligfield, "Heart Disease: A textbook of Cardiovascular Medicine, 5/E, edited by Eugene Braunwald, W.B. Saunders, Philadelphia (1997) 2143 pages, illustrated, $125.00 ISBN: 9-7216-5666-8," *Clin. Cardiol.*, vol. 21, no. 2, pp. 147–148, Feb. 2010.

[4] M. Arif, I. A. Malagore, and F. A. Afsar, "Detection and localization of myocardial infarction using K-nearest neighbor classifier," *J. Med. Syst.*, vol. 36, no. 1, pp. 279–289, 2012.

[5] L. N. Sharma, R. K. Tripathy, and S. Dandapat, "Multiscale energy and eigenspace approach to detection and localization of myocardial infarction," *IEEE Trans. Biomed. Eng.*, vol. 62, no. 7, pp. 1827–1837, Jul. 2015.

[6] L. Sun, Y. Lu, K. Yang, and S. Li, "ECG analysis using multiple instance learning for myocardial infarction detection," *IEEE Trans. Biomed. Eng.*, vol. 59, no. 12, pp. 3348–3356, Dec. 2012.

[7] U. R. Acharya, H. Fujita, V. K. Sudarshan, S. L. Oh, M. Adam, J. E. W. Koh, J. H. Tan, D. N. Ghista, R. J. Martis, C. K. Chua, C. K. Poo, and R. S. Tan, "Automated detection and localization of myocardial infarction using electrocardiogram: A comparative study of different leads," *Knowl. Based Syst.*, vol. 99, pp. 146–156, May 2016.

[8] R. K. Tripathy, A. Bhattacharyya, and R. B. Pachori, "A novel approach for detection of myocardial infarction from ECG signals of multiple electrodes," *IEEE Sensors J.*, vol. 19, no. 2, pp. 4509–4517, Jun. 2019.

[9] R. K. Tripathy, A. Bhattacharyya, and R. B. Pachori, "Localization of myocardial infarction from multi-lead ecg signals using multiscale analysis and convolutional neural network," *IEEE Sensors J.*, vol. 19, no. 23, pp. 11437–11448, Dec. 2019.

[10] B. Liu, J. Liu, G. Wang, K. Huang, F. Li, Y. Zheng, Y. Luo, and F. Zhou, "A novel electrocardiogram parameterization algorithm and its application in myocardial infarction detection," *Comput. Biol. Med.*, vol. 61, pp. 178–184, Jun. 2015.

[11] R. K. Tripathy and S. Dandapat, "Detection of myocardial infarction from vectorcardiogram using relevance vector machine," *Signal, Image Video Process.*, vol. 11, no. 6, pp. 1139–1146, 2017.

[12] G. Bortolan and I. Christov, "Myocardial infarction and ischemia characterization from T-loop morphology in VCG," in *Proc. Comput. Cardiol.*, Sep. 2001, pp. 633–636.

[13] K. Thygesen, J. S. Alpert, A. S. Jaffe, M. L. Simoons, B. R. Chaitman, and H. D. White, "Third universal definition of myocardial infarction," *Glob. Heart*, vol. 7, no. 4, pp. 275–295, 2012.

[14] M. Kumar, R. B. Pachori, and U. R. Acharya, "Automated diagnosis of myocardial infarction ECG signals using sample entropy in flexible analytic wavelet transform framework," *Entropy*, vol. 19, no. 9, p. 488, Sep. 2017.

[15] R. K. Tripathy, L. N. Sharma, and S. Dandapat, "A new way of quantifying diagnostic information from multilead electrocardiogram for cardiac disease classification," *Healthc. Technol. Lett.*, vol. 1, no. 4, pp. 98–103, Oct. 2014.
[16] C. Han and L. Shi, "Automated interpretable detection of myocardial infarction fusing energy entropy and morphological features," *Comput. Methods Programs Biomed.*, vol. 175, pp. 9–23, Jul. 2019.
[17] M. Sharma, R. San Tan, and U. R. Acharya, "A novel automated diagnostic system for classification of myocardial infarction ECG signals using an optimal biorthogonal filter bank," *Comput. Biol. Med.*, vol. 102, pp. 341–356, Nov. 2018.
[18] U. R. Acharya, H. Fujita, V. K. Sudarshan, S. L. Oh, M. Adam, J. H. Tan, J. H. Koo, A. Jain, and C. M. Lim, and K. C. Chua, "Automated characterization of coronary artery disease, myocardial infarction, and congestive heart failure using contourlet and shearlet transforms of electrocardiogram signal," *Knowl. Based Syst.*, vol. 132, pp. 156–166, Sep. 2017.
[19] E. S. Jayachandran, "Analysis of myocardial infarction using discrete wavelet transform," *J. Med. Syst.*, vol. 34, no. 6, pp. 985–992, 2010.
[20] N. Safdarian, N. J. Dabanloo, and G. Attarodi, "A new pattern recognition method for detection and localization of myocardial infarction using T-wave integral and total integral as extracted features from one cycle of ECG signal," *J. Biomed. Sci. Eng.*, vol. 07, no. 10, pp. 818–824, Aug. 2014.
[21] J. Schmidhuber, "Deep Learning in neural networks: An overview," *Neural Netw.*, vol. 61, pp. 85–117, Jan. 2015.
[22] G. E. Hinton, S. Osindero, and Y.-W. Teh, "A fast learning algorithm for deep belief nets," *Neural Comput.*, vol. 18, no. 7, pp. 1527–1554, 2006.
[23] A. Graves, M. Liwicki, S. Fernández, R. Bertolami, H. Bunke, and J. Schmidhuber, "A novel connectionist system for unconstrained handwriting recognition," *IEEE Trans. Pattern Anal. Mach. Intell.*, vol. 31, no. 5, pp. 855–868, May 2009.
[24] K. Fukushima, "Neocognitron: A self-organizing neural network model for a mechanism of pattern recognition unaffected by shift in position," *Biol. Cybern.*, vol. 36, no. 4, pp. 193–202, Apr. 1980.
[25] B. S. Aaron van den Oord and S. Dieleman, "Deep content-based music recommendation Aäron," in *Proc. IT-Risiko-Manage. Mit Syst.*, 2006, pp. 109–121.
[26] D. Ciregan, U. Meier, and J. Schmidhuber, "Multi-column deep neural networks for image classification," in *Proc. IEEE Conf. Comput. Vis. Pattern Recognit.*, Jun. 2012, pp. 3642–3649.
[27] R. Collobert and J. Weston, "A unified architecture for natural language processing: Deep neural networks with multitask learning," in *Proc. Int. Conf. Mach. Learn.*, Jul. 2008, pp. 160–167.
[28] U. B. Baloglu, M. Talo, O. Yildirim, R. S. Tan, and U. R. Acharya, "Classification of myocardial infarction with multi-lead ECG signals and deep CNN," *Pattern Recognit. Lett.*, vol. 122, pp. 23–30, May 2019.
[29] T. Reasat and C. Shahnaz, "Detection of inferior myocardial infarction using shallow convolutional neural networks," in *Proc. 5th IEEE Reg. Humanit. Technol. Conf. (R10-HTC)*, Dec. 2017, pp. 718–721.
[30] W. Liu, F. Wang, Q. Huang, S. Chang, H. Wang, and J. He, "MFB-CBRNN: A hybrid network for MI detection using 12-lead ECGs," *IEEE J. Biomed. Heal. Informat.*, to be published.
[31] C. Han and L. Shi, "ML–ResNet: A novel network to detect and locate myocardial infarction using 12 leads ECG," *Comput. Methods Programs Biomed.*, vol. 185, Mar. 2020, Art. no. 105138.
[32] W. Liu, Q. Huang, S. Chang, H. Wang, and J. He, "Multiple-feature-branch convolutional neural network for myocardial infarction diagnosis using electrocardiogram," *Biomed. Signal Process. Control*, vol. 45, pp. 22–32, Aug. 2018.
[33] W. Liu, M. Zhang, Y. Zhang, Y. Liao, Q. Huang, S. Chang, H. Wang, and J. He, "Real-time multilead convolutional neural network for myocardial infarction detection," *IEEE J. Biomed. Health Inform.*, vol. 22, no. 5, pp. 1434–1444, Sep. 2018.
[34] K. Feng, X. Pi, H. Liu, and K. Sun, "Myocardial infarction classification based on convolutional neural network and recurrent neural network," *Appl. Sci.*, vol. 9, no. 9, p. 1879, May 2019.
[35] R. Miotto, F. Wang, S. Wang, X. Jiang, and J. T. Dudley, "Deep learning for healthcare: Review, opportunities and challenges," *Brief. Bioinform.*, vol. 19, no. 6, pp. 1236–1246, Nov. 2018.
[36] T.-H. Chan, K. Jia, S. Gao, J. Lu, and Z. Zeng, Y. Ma, "PCANet: A simple deep learning baseline for image classification?" *IEEE Trans. Image Process*, vol. 24, no. 12, pp. 5017–5032, Dec. 2015.
[37] J.-N. Lee, Y.-H. Byeon, S.-B. Pan, and K.-C. Kwak, "An eigen ECG network approach based on PCANet for personal identification from ECG signal," *Sensors*, vol. 18, no. 11, p. 4024, Nov. 2018.
[38] D. F. Silva, V. M. A. D. Souza, and G. E. A. P. A. Batista, "Time series classification using compression distance of recurrence plots," in *Proc. IEEE 13th Int. Conf. Data Mining*, Dec. 2013, pp. 687–696.
[39] R. V. Donner, Y. Zou, J. F. Donges, N. Marwan, and J. Kurths, "Recurrence networks—A novel paradigm for nonlinear time series analysis," *New J. Phys.*, vol. 12, Mar. 2010, Art. no. 033025.
[40] U. R. Acharya, H. Fujita, S. L. Oh, Y. Hagiwara, J. H. Tan, and M. Adam, "Application of deep convolutional neural network for automated detection of myocardial infarction using ECG signals," *Inf. Sci.*, vols. 415–416, pp. 190–198, Nov. 2017.
[41] A. L. Goldberger, L. A. Amaral, L. Glass, J. M. Hausdorff, P. C. Ivanov, R. G. Mark, J. E. Mietus, G. B. Moody, C. K. Peng, and H. E. Stanley, "PhysioBank, PhysioToolkit, and PhysioNet: Components of a new research resource for complex physiologic signals," *Circulation*, vol. 101, no. 23, p. e215, Jun. 2000.
[42] U. R. Acharya, H. Fujita, M. Adam, O. S. Lih, V. K. Sudarshan, T. J. Hong, J. E. Koh, Y. Hagiwara, C. K. Chua, C. K. Poo, and T. R. San, "Automated characterization and classification of coronary artery disease and myocardial infarction by decomposition of ECG signals: A comparative study," *Inf. Sci.*, vol. 377, pp. 17–29, Jan. 2017.
[43] D. P. Tobon and T. H. Falk, "Adaptive spectro-temporal filtering for electrocardiogram signal enhancement," *IEEE J. Biomed. Heal. Informat.*, vol. 22, no. 2, pp. 421–428, Mar. 2018.
[44] S. K. Yadav, R. Sinha, and P. K. Bora, "Electrocardiogram signal denoising using non-local wavelet transform domain filtering," *IET Signal Process.*, vol. 9, no. 1, pp. 88–96, Feb. 2015.
[45] R. R. Sharma and R. B. Pachori, "Baseline wander and power line interference removal from ECG signals using eigenvalue decomposition," *Biomed. Signal Process. Control*, vol. 45, pp. 33–49, Aug. 2018.
[46] B. N. Singh and A. K. Tiwari, "Optimal selection of wavelet basis function applied to ECG signal denoising," *Digit. Signal Process.*, vol. 16, no. 3, pp. 275–287, May 2006.
[47] J. Pan and W. J. Tompkins, "A real-time QRS detection algorithm," *IEEE Trans. Biomed. Eng.*, vol. 32, no. 3, pp. 230–236, Mar. 2007.
[48] Z. Wang and T. Oates, "Imaging time-series to improve classification and imputation," in *Proc. IJCAI Int. Jt. Conf. Artif. Intell.*, Jun. 2015, pp. 3939–3945.
[49] N. Hatami, Y. Gavet, and J. Debayle, "Classification of time-series images using deep convolutional neural networks," *Proc. SPIE*, Apr. 2017, Art. no. 106960Y.
[50] C. Cortes and V. Vapnik, "Support-vector networks," *Mach. Learn.*, vol. 20, no. 3, pp. 273–297, Sep. 1995.
[51] W. S. Rayens, "Discriminant analysis and statistical pattern recognition," *J. Royal Stat. Soc.*, vol. 35, no. 3, pp. 324–326, 2010.
[52] D. E. Rumelhart, G. E. Hinton, and R. J. Williams, "Learning representations by back-propagating errors," *Nature*, vol. 323, pp. 533–536, Oct. 1986.
[53] T. K. Ho, "The random subspace method for constructing decision forests," *IEEE Trans. Pattern Anal. Mach. Intell.*, vol. 20, no. 8, pp. 832–844, Aug. 1998.
[54] D. Wang, Y. Si, W. Yang, G. Zhang, and T. Liu, "A novel heart rate robust method for short-term electrocardiogram biometric identification," *Appl. Sci.*, vol. 9, no. 1, p. 201, Jan. 2019.
[55] Y. H. Hu, S. Palreddy, and W. J. Tompkins, "A patient-adaptable ECG beat classifier using a mixture of experts approach," *IEEE Trans. Biomed. Eng.*, vol. 44, no. 9, pp. 891–900, Sep. 1997.
[56] S. Kiranyaz, T. Ince, and M. Gabbouj, "Real-time patient-specific ECG classification by 1-D convolutional neural networks," *IEEE Trans. Biomed. Eng.*, vol. 63, no. 3, pp. 664–675, Mar. 2016.

GONG ZHANG received the master's degree in circuits and systems from South China Normal University, Guangzhou, China, in 2014. He is currently pursuing the Ph.D. degree with the College of Communication Engineering, Jilin University, China. His research interests include biomedical signal processing and recognition. His current research focuses on ECG biometric identification and recognition.

YUJUAN SI received the master's and Ph.D. degrees in engineering from the Jilin University of Technology, in 1988 and 1996, respectively. She is currently a Professor with the Institute of Communication Engineering, Jilin University. Her research interests include embedded systems and biomedical signal processing and recognition.

DI WANG received the master's degree in signal and information processing from Jilin University, Changchun, China, in 2016. He is currently pursuing the Ph.D. degree with the College of Communication Engineering, Jilin University, China. His research interests include biomedical signal processing and recognition. His current research focuses on ECG biometric identification and recognition.

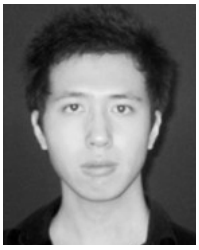

WEIYI YANG was born in Liaoning, China. He received the bachelor's degree from Jilin University, in 2017, where he is currently pursuing the Ph.D. degree. His research interests include biomedical signal processing and recognition. His current research focuses on ECG recognition.

YONGJIAN SUN was born in Guangdong, China. He received the bachelor's degree from Jilin University, in 2014. He is currently with the Zhuhai College of Jilin University. His research interests include biomedical signal processing and recognition. His current research focuses on ECG recognition and FPGA simulation.